International Journal of Computer Vision 24(2), 125–135 (1997)

Shape from Shading with Interreflections Under a Proximal Light Source: Distortion-Free Copying of an Unfolded Book

TOSHIKAZU WADA[†], HIROYUKI UKIDA[‡] AND TAKASHI MATSUYAMA[*]
Department of Information Technology, Faculty of Engineering, Okayama University, 3-1-1, Tsushima Naka, Okayama 700, Japan
twada@kuee.kyoto-u.ac.jp
ukida@me.tokushima-u.ac.jp
tm@kuee.kyoto-u.ac.jp

Received August, 1995; Accepted September, 1995

Abstract. We address the problem of recovering the 3D shape of an unfolded book surface from the shading information in a scanner image. This shape-from-shading problem in a real world environment is made difficult by a proximal, moving light source, interreflections, specular reflections, and a nonuniform albedo distribution. Taking all these factors into account, we formulate the problem as an iterative, non-linear optimization problem. Piecewise polynomial models of the 3D shape and albedo distribution are introduced to efficiently and stably compute the shape in practice. Finally, we propose a method to restore the distorted scanner image based on the reconstructed 3D shape. The image restoration experiments for real book surfaces demonstrate that much of the geometric and photometric distortions are removed by our method.

1. Introduction

In this paper, we address the problem of recovering the 3D shape of an unfolded book surface from the shading information in a scanner image. This shape-from-shading problem in a real world environment is made difficult by the following characteristics:

- *Proximal Light Source*: The light source of an image scanner is located very close to the book surface. This implies that the illuminant intensity and the light source direction varies with respect to the location on the book surface.
- *Interreflections*: The light reflected on one side of an unfolded book surface illuminates the other.
- *Moving Light Source*: The light source moves during the scanning process.
- *Specular Reflections*: The book surface is not Lambertian.
- *Nonuniform Albedo Distribution*: The albedo distribution over a printed book surface is not uniform.

In the following sections, we formulate this real world shape-from-shading problem based on an iterative, non-linear optimization scheme. Piecewise polynomial models of the 3D shape and albedo distribution are introduced to efficiently and stably compute the shape in practice. We also propose a method of restoring the distorted scanner image based on the reconstructed 3D shape and demonstrate the effectiveness and efficiency of the proposed methods with several experiments using scanner images of real books.

2. Problem Formulation

First, let us consider an *ideal* shape-from-shading problem. Ideally, the following conditions would be satisfied:

[†]Department of Electronics and Communication, Kyoto University.
[‡]Department of Machinery, Tokushima University.
[*]Department of Electronics and Communication, Kyoto University, Sakyo, Kyoto 606-01, Japan.

- *Distant Light Source*: This implies that the illuminant intensity and the light source direction are constant over the object surface.
- *No Interreflections*: The object surface is illuminated only by the the light source.
- *Fixed Light Source Position*
- *Lambertian Surface*
- *Constant Albedos*: The albedo distribution is uniform over the object surface.

The problem under these ideal conditions can be formulated as:

$$I_o(\boldsymbol{x}) = \rho I_s \cos\varphi(\boldsymbol{x}), \tag{1}$$

where $\boldsymbol{x}$ denotes a 2D point in the image, $I_o(\boldsymbol{x})$ the reflected light intensity observed at $\boldsymbol{x}$, I_s the illuminant intensity, ρ the albedo on the surface, and $\varphi(\boldsymbol{x})$ the angle between the light source direction and the surface normal at the 3D point on the object surface corresponding to $\boldsymbol{x}$.

In this case, $\varphi(\boldsymbol{x})$ can easily be calculated for given $\rho\, I_s$.[1] Then, the shape (i.e., surface normals) of the object surface can be computed from $\varphi(\boldsymbol{x})$ by introducing additional constraints such as those from photometric stereo (Woodham, 1981) or the assumption of smooth (Ikeuchi, 1982) or cylindrical (Asada, 1987) surfaces.

Now, we describe a formulation of our shape-from-shading problem under the real world characteristics described in the introduction. We begin from the ideal formulation of Eq. (1) and modify the formulation step by step to account for the characteristics of our real world problem.

2.1. *Proximal Light Source*

With a proximal light source, the illuminant intensity is no longer constant over the object surface. The illuminant intensity is now a function of the location of the object surface and that of the light source. We can formulate the problem as follows:

$$I_o(\boldsymbol{x}) = \rho\, I_s(\boldsymbol{s}(\boldsymbol{x}), \boldsymbol{l})\, \cos\varphi(\boldsymbol{x}), \tag{2}$$

where $\boldsymbol{l}$ denotes the 3D location of the light source, $\boldsymbol{s}(\boldsymbol{x})$ the 3D point on the object surface corresponding to $\boldsymbol{x}$. Notice that the absolute location (depth) of the object surface $\boldsymbol{s}(\boldsymbol{x})$ is required to compute $\varphi(\boldsymbol{x})$. The proximal light source transforms the *shape*-from-shading problem into the *depth*-from-shading problem.

2.2. *Interreflections*

The problem under interreflection is formulated by Nayar et al. (1990), as:

$$I_o(\boldsymbol{x}) = \rho \left\{ I_s + \int \frac{I_o(\boldsymbol{x}')}{d^2(\boldsymbol{s}(\boldsymbol{x}), \boldsymbol{s}(\boldsymbol{x}'))} d\boldsymbol{x}' \right\} \cos\varphi(\boldsymbol{x}), \tag{3}$$

where $d(\boldsymbol{s}(\boldsymbol{x}), \boldsymbol{s}(\boldsymbol{x}'))$ denotes the distance between $\boldsymbol{s}(\boldsymbol{x})$ and $\boldsymbol{s}(\boldsymbol{x}')$. In this formulation, we assume that 1) the light reflected at $\boldsymbol{s}(\boldsymbol{x}')$ can reach $\boldsymbol{s}(\boldsymbol{x})$ for any combinations of $\boldsymbol{x}$ and $\boldsymbol{x}'$ and 2) the light reflected more than twice is sufficiently attenuated to be neglected. Note that with interreflections, the *global shape* of the object surface ($\forall \boldsymbol{x}'\ d(\boldsymbol{s}(\boldsymbol{x}), \boldsymbol{s}(\boldsymbol{x}'))$) is required to compute $\varphi(\boldsymbol{x})$.

2.3. *Interreflections Under Proximal Light Source*

Combining the proximal light source and interreflections into one equation, we have:

$$I_o(\boldsymbol{x}) = \rho \left\{ I_s(\boldsymbol{s}(\boldsymbol{x}), \boldsymbol{l}) + \int \frac{I_o(\boldsymbol{x}')}{d^2(\boldsymbol{s}(\boldsymbol{x}), \boldsymbol{s}(\boldsymbol{x}'))} d\boldsymbol{x}' \right\} \times \cos\varphi(\boldsymbol{x}). \tag{4}$$

In this case, the *overall depth* of the object surface ($\forall \boldsymbol{x}\ \boldsymbol{s}(\boldsymbol{x})$) is required to compute $\varphi(\boldsymbol{x})$.

2.4. *Moving Light Source*

Introducing a moving light source[2] into Eq. (4), the problem can be formulated as:

$$I_o(\boldsymbol{x}) = \rho \left\{ I_s(\boldsymbol{s}(\boldsymbol{x}), \boldsymbol{l}(\boldsymbol{x})) + \int \frac{I_o'(\boldsymbol{s}(\boldsymbol{x}'), \boldsymbol{l}(\boldsymbol{x}))}{d^2(\boldsymbol{s}(\boldsymbol{x}), \boldsymbol{s}(\boldsymbol{x}'))} d\boldsymbol{x}' \right\} \times \cos\varphi(\boldsymbol{x}), \tag{5}$$

where $I_o'(\boldsymbol{s}(\boldsymbol{x}'), \boldsymbol{l}(\boldsymbol{x}))$ is the reflected light intensity at $\boldsymbol{s}(\boldsymbol{x}')$:

$$I_o'(\boldsymbol{s}(\boldsymbol{x}'), \boldsymbol{l}(\boldsymbol{x})) = \rho I_s(\boldsymbol{s}(\boldsymbol{x}'), \boldsymbol{l}(\boldsymbol{x})) \cos\varphi(\boldsymbol{x}') \tag{6}$$

and $\boldsymbol{l}(\boldsymbol{x})$ denotes the light source location corresponding to $\boldsymbol{x}$. Under the moving light source, $I_o'(\boldsymbol{s}(\boldsymbol{x}'), \boldsymbol{l}(\boldsymbol{x}))$ must be calculated at each point on the object surface. Hence, the computation becomes more expensive than that under a fixed light source (Nayar et al., 1990).

2.5. The Complete Formulation

Finally, we can formulate our problem by incorporating specular reflection and nonuniform albedo distribution characteristics into Eq. (5):

$$I_o(\boldsymbol{x}) = \left\{ I_s(\boldsymbol{s}(\boldsymbol{x}), \boldsymbol{l}(\boldsymbol{x})) + \int \frac{I_o'(\boldsymbol{s}(\boldsymbol{x}'), \boldsymbol{l}(\boldsymbol{x}))}{d^2(\boldsymbol{s}(\boldsymbol{x}), \boldsymbol{s}(\boldsymbol{x}'))} d\boldsymbol{x}' \right\} \times \rho(\boldsymbol{s}(\boldsymbol{x})) f(\varphi(\boldsymbol{x}), \boldsymbol{s}(\boldsymbol{x})), \tag{7}$$

where

$$I_o'(\boldsymbol{s}(\boldsymbol{x}'), \boldsymbol{l}(\boldsymbol{x})) = \rho(\boldsymbol{s}(\boldsymbol{x}')) I_s(\boldsymbol{s}(\boldsymbol{x}'), \boldsymbol{l}(\boldsymbol{x})) \times f(\varphi(\boldsymbol{x}'), \boldsymbol{s}(\boldsymbol{x}')), \tag{8}$$

$\rho(\boldsymbol{s}(\boldsymbol{x}))$ denotes the albedo and $f(\varphi(\boldsymbol{x}), \boldsymbol{s}(\boldsymbol{x}))$ is the reflectance property at $\boldsymbol{s}(\boldsymbol{x})$. In this problem, the *global shape* and *overall albedo distribution* on the object surface ($\forall \boldsymbol{x}\ \boldsymbol{s}(\boldsymbol{x})$ and $\forall \boldsymbol{x}\ \rho(\boldsymbol{s}(\boldsymbol{x}))$) are required to compute $\varphi(\boldsymbol{x})$.

3. Solution Scheme

To solve our problem, we must compute the absolute shape ($\forall \boldsymbol{x}\ \boldsymbol{s}(\boldsymbol{x})$) and albedos ($\forall \boldsymbol{x}\ \rho(\boldsymbol{s}(\boldsymbol{x}))$) from an observed scanner image. To attack this complicated problem, we assume that light source location $\boldsymbol{l}(\boldsymbol{x})$, illuminant intensity $I_s(\boldsymbol{s}, \boldsymbol{l})$ and reflectance ratio $f(\varphi, \boldsymbol{s})$ are known a priori. This assumption is practical because the first two functions represent optical properties of the image scanner and the latter the intrinsic property of the printed paper to be scanned, all of which can be calibrated a priori.

Equation (7) can be rewritten as a sum of the direct reflection and interreflection:

$$I_o(\boldsymbol{s}, \varphi, \rho) = \rho\, \{I_{\text{dir}}(\boldsymbol{s}, \varphi) + I_{\text{inter}}(\boldsymbol{s}, \varphi, \rho)\}, \tag{9}$$

where

$$I_{\text{dir}}(\boldsymbol{s}, \varphi) = f(\varphi(\boldsymbol{x}), \boldsymbol{s}(\boldsymbol{x})) I_s(\boldsymbol{s}(\boldsymbol{x}), \boldsymbol{l}(\boldsymbol{x})) \tag{10}$$

$$I_{\text{inter}}(\boldsymbol{s}, \varphi, \rho) = f(\varphi(\boldsymbol{x}), \boldsymbol{s}(\boldsymbol{x})) \times \int \frac{I_o'(\boldsymbol{s}(\boldsymbol{x}'), \boldsymbol{l}(\boldsymbol{x}))}{d^2(\boldsymbol{s}(\boldsymbol{x}), \boldsymbol{s}(\boldsymbol{x}'))} d\boldsymbol{x}'. \tag{11}$$

Using these notations and assumptions, we discuss why and how this problem can be solved.

3.1. Uniqueness of the Solution

The assumptions mentioned above reduce the number of unknown parameter functions of our problem to three: depth $\boldsymbol{s}$, shape φ and albedo distribution ρ of the object surface. The problem to be solved can be formulated as that of finding $\boldsymbol{s}$, φ and ρ which minimize the following objective functional:

$$\begin{aligned} F(\boldsymbol{s}, \varphi, \rho) &= \|I_o(\boldsymbol{s}, \varphi, \rho) - I_o^*\|^2 \\ &= \|\rho\, \{I_{\text{dir}}(\boldsymbol{s}, \varphi) + I_{\text{inter}}(\boldsymbol{s}, \varphi, \rho)\} - I_o^*\|^2, \end{aligned} \tag{12}$$

where I_o^* represents the observed intensity.

If the I_o that minimizes F is unique and its inverse mapping exists, then the solutions $\boldsymbol{s}(\boldsymbol{x})$, $\varphi(\boldsymbol{x})$ and $\rho(\boldsymbol{s}(\boldsymbol{x}))$ are unique.

The first condition, that the I_o which minimizes F is unique, is satisfied for the following reason: at the end of the optimization process, $I_o(\boldsymbol{s}, \varphi, \rho)$ should be approximately equal to the observed intensity I_o^*. Hence, $I_o(\boldsymbol{s}, \varphi, \rho)$ in Eq. (9) can be substituted by I_o^*, and we obtain the following equation[3]:

$$\rho = \frac{I_o^*}{I_{\text{dir}}(\boldsymbol{s}, \varphi) + I_{\text{inter}}(\boldsymbol{s}, \varphi, \rho)}. \tag{13}$$

In the case of no interreflections, the optimal ρ is represented by $\rho = I_o^* / I_{\text{direct}}(\boldsymbol{s}, \varphi)$ which makes $F = 0$. That is, the optimal I_o is uniquely determined as I_o^*.

However, the second condition is not satisfied, since an optimal solution of ρ described above exists for many combinations of $\boldsymbol{s}$ and φ. That is, the mapping from $(\boldsymbol{s}, \varphi, \rho)$ to I_o^* is many-to-one, i.e., the inverse mapping does not exist. Thus, no unique solution, $(\boldsymbol{s}, \varphi, \rho)$, minimizes Eq. (12).

For a unique solution, a mapping from I_o^* to $(\boldsymbol{s}, \varphi, \rho)$ is necessary. To guarantee it, the degrees of freedom of shape and albedos must be reduced. To accomplish this, we introduce the following constraints:

- We assume that the object surface is uniquely defined by a 3D curve $\boldsymbol{s}(\boldsymbol{x}(u))$, where $\boldsymbol{x}(u)$ is a 2D curve in the image plane. The ruled surface[4] is a typical example of such surfaces. Under this constraint, $\boldsymbol{s}(\boldsymbol{x})$ is uniquely determined by a curve $\boldsymbol{s}_u = \boldsymbol{s}(\boldsymbol{x}(u))$. That is, $\boldsymbol{s}$ can be represented as:

$$\boldsymbol{s} = \boldsymbol{s}(\boldsymbol{s}_u). \tag{14}$$

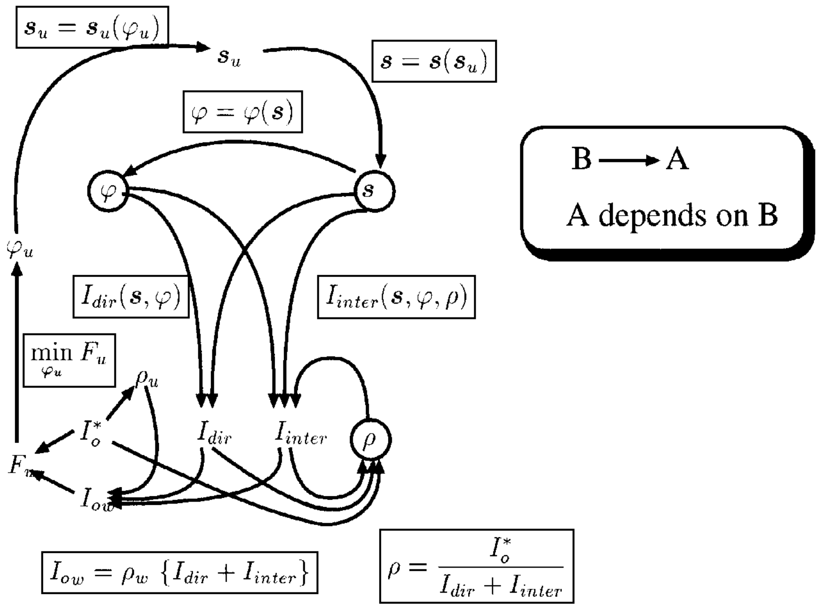

Figure 1. Structure of the problem.

- We also assume that $\boldsymbol{x}(u)$ and the albedos $\rho_u = \rho(\boldsymbol{s}_u)$ can be computed from I_o^*.
- If the object has a smooth surface, $\boldsymbol{s}$ and φ depend on each other. We assume that the depth of a certain point (at least one point) on the object surface is known and the surface is smooth. Under these assumptions, $\boldsymbol{s}$ and φ can be represented as:

$$\boldsymbol{s} = \boldsymbol{s}(\varphi), \qquad \varphi = \varphi(\boldsymbol{s}). \tag{15}$$

Also, $\boldsymbol{s}_u$ and $\varphi_u = \varphi(\boldsymbol{x}(u))$ depend on each other:

$$\boldsymbol{s}_u = \boldsymbol{s}_u(\varphi_u), \qquad \varphi_u = \varphi_u(\boldsymbol{s}_u). \tag{16}$$

Figure 1 shows the dependencies among the variables.

Under these assumptions, the independent argument of I_o is reduced to a function of one variable: Since, we can compute $\boldsymbol{s}$ given φ, φ can be computed from φ_u (ruled surface assumption), and ρ depends on φ and $\boldsymbol{s}$ then, the independent argument of I_o is simply φ_u.[5]

The original problem is reduced to computing an optimal φ_u which minimizes the total square error between I_o and I_o^* on $\boldsymbol{x}(u)$. That is, a new objective functional on the reduced domain $\boldsymbol{x}(u)$ is introduced. To distinguish it from F, it is denoted by F_u. Also, I_o and I_o^* on $\boldsymbol{x}(u)$ are denoted by I_{ou} and I_{ou}^* respectively.

If the following condition is satisfied, there is a unique mapping from I_{ou}^* to φ_u and the the optimal solution is uniquely determined:

$$I_{ou}(\varphi_{u1}) = I_{ou}(\varphi_{u2}) = I_{ou}^* \Rightarrow \varphi_{u1} = \varphi_{u2}. \tag{17}$$

Since φ_u and I_{ou} are both 1D functions having the same degree of freedom, the optimal φ_u which makes $I_{ou} = I_o^*$ is expected to be unique[6]. For example, if ρ_u and I_{ou}^* are constant and $\boldsymbol{s}_u(\varphi_{u1})$ is a planar curve, $\boldsymbol{s}_u(\varphi_{u2})$ cannot be a planar curve and $I_{ou}(\varphi_{u2})$ must be shaded. Hence, the condition mentioned above is satisfied in this case. If the mapping does not exist in some cases, the uniqueness of the solution is not guaranteed but the number of optimal solutions must be reduced by the assumptions introduced in this section.

3.2. *Algorithm*

As discussed above, the number of optimal solution is reduced by the assumptions described above and the uniqueness is guaranteed for some cases. Here we discuss the computation of the optimal φ_u which determines the optimal values of φ, $\boldsymbol{s}$ and ρ.

In practice, the value of $F_u(\varphi_u)$ cannot be directly computed from its argument φ_u, because I_{inter} in Eq. (11) and ρ in Eq. (13) mutually depend on each other and the mutual dependency cannot be solved algebraicly. Such difficulty, which is essentially caused by the presence of interreflections, keeps us from solving the problem by ordinary optimization algorithms. It leads us to the iterative solution technique.

For the numerical computation of ρ and I_{inter}, we decompose Eq. (13) into two equations:

$$I_{\text{inter}} = I_{\text{inter}}(\boldsymbol{s}, \varphi, \rho), \tag{18}$$

$$\rho = \rho(\boldsymbol{s}, \varphi, I_{\text{inter}}) = \frac{I_o^*}{I_{\text{dir}}(\boldsymbol{s}, \varphi) + I_{\text{inter}}}. \tag{19}$$

One way to compute I_{inter} and ρ is to compute Eqs. (11) and (19) iteratively for fixed values $\boldsymbol{s}$ and φ. This computation scheme is the same as that proposed in (Nayar et al. 1990), which is considered as a procedure to compute I_{inter} and ρ from $\boldsymbol{s}$ and φ.

To compute the optimal $\boldsymbol{s}$, φ and ρ simultaneously, we embed the optimization procedure for $\min_{\varphi_u} F_u$ into the above iterative procedure and obtain the following algorithm:

Initial estimate: Extract $\boldsymbol{x}(u)$ and compute ρ_u from I_o^*. Also, estimate the initial values of $\boldsymbol{s}$, φ and ρ by neglecting the term I_{inter}.

Step 1: Compute I_{inter} from the estimated $\boldsymbol{s}$, φ and ρ.

Step 2: Compute φ_u which minimizes the objective functional F_u using estimated I_{inter}. Also, compute $\boldsymbol{s}$ and φ from φ_u.

Step 3: Compute ρ using the estimated $\boldsymbol{s}$, φ and I_{inter}.

Step 4: If the objective functional exceeds the given threshold then goto **Step 1**. Otherwise stop.

The detailed algorithm is described in Section 5.2.

4. Practical Model of Copying an Unfolded Book

We discussed the basic solution scheme of our problem to compute the shape, depth and albedo distribution of the unfolded book surface. Here we specify our problem by describing the practical conditions of copying an unfolded book surface by an image scanner.

4.1. Geometric Models

Figure 2 shows the structure of the image scanner and the coordinate system of our problem. The image

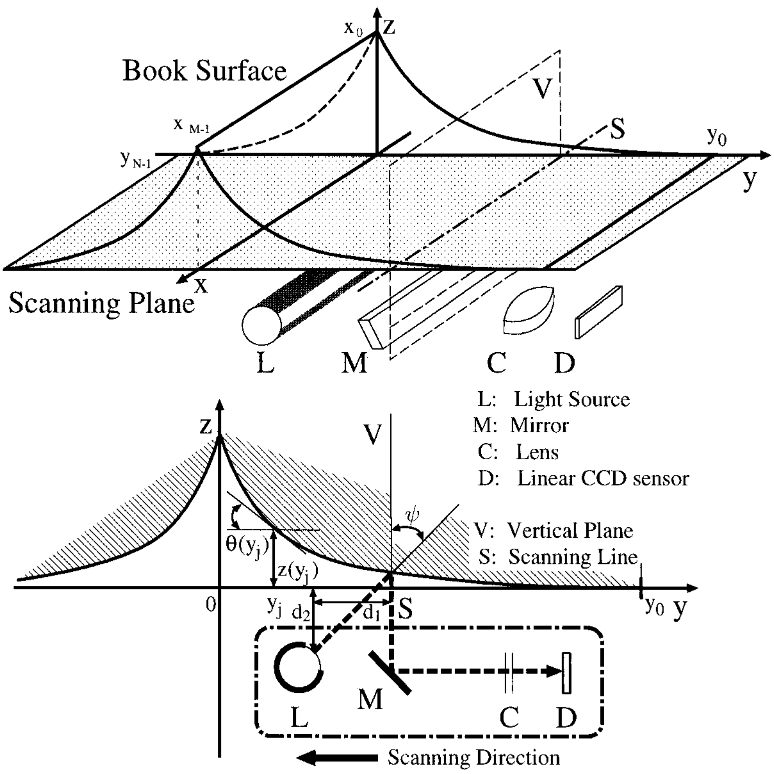

Figure 2. Configuration of image scanner and book surface.

scanner consists of light source L, linear CCD sensor D, mirror M and lens C. The sensor D takes a 1D image $P^*(x_i)$ along the scanning line S and moves with L, M, and C. The sequence $P^*(x_i)$ forms a 2D image $P^*(x_i, y_j)$. Note that while $P^*(x_i)$ is obtained by perspective projection, the projection along the y-axis is equivalent to the orthogonal projection.

We describe the geometric configuration of the book surface to specify the assumptions which is introduced in Section 3.1:

- The book surface is cylindrical (constant cross section)[7] and its cross section shape on the y-z plane is smooth except for the point separating the book pages.
- The unfolded book surface is aligned on the scanning plane so that the center line separating the book pages is parallel to and lies just above the x-axis. Hence, the cross section is constant along the x-axis.
- Both ends of the book surface touch the scanning plane. That is, we can neglect the term I_{inter} in Eq. (13) and albedos can be estimated at the ends of the book surface without iterative computation.

With these assumptions, φ and $\boldsymbol{s}$ are reduced to 1D functions of y.

4.2. Optical Model

The relationship between the image intensity (pixel value) and the reflected light intensity is represented as follows:

$$\begin{aligned} P(x_i, y_j) &= \alpha I_o(x_i, y_j) + \beta \\ &= \alpha\rho(x_i, y_j)\{I_{\text{dir}}(x_i, y_j) + I_{\text{inter}}(x_i, y_j)\} + \beta, \end{aligned} \tag{20}$$

where

- $P(x_i, y_j)$: The image intensity at (x_i, y_j) in the observed image.
- α, β: Gain and the bias of the photoelectric transformation in the image scanner respectively.
- $I_{\text{dir}}(x_i, y_j)$: The reflected light component corresponding to the direct illumination from the light source.
- $I_{\text{inter}}(x_i, y_j)$: The reflected light component corresponding to the indirect illumination from the opposite side of the book surface.

$I_{\text{dir}}(x_i, y_j)$ and $I_{\text{inter}}(x_i, y_j)$ are represented as follows:

$$I_{\text{dir}}(x_i, y_j) = I_s(y_j, z(y_j), y_j)\ f(\boldsymbol{n}_1, \boldsymbol{l}_1, \boldsymbol{v}_1), \tag{21}$$

$$\begin{aligned} I_{\text{inter}}(x_i, y_j) &= A \sum_{y_n=y_0}^{y_{N-1}} \Bigg[V(y_n, y_j)\ I_s(y_n, z(y_n), y_j) \\ &\quad \times \sum_{x_m=x_0}^{x_{M-1}} \rho(x_m, y_n) \frac{f(\boldsymbol{n}_2, \boldsymbol{l}_2, \boldsymbol{v}_2)\, f(\boldsymbol{n}_1, \boldsymbol{l}_3, \boldsymbol{v}_1)}{d^2(x_m, y_n, x_i, y_j)} \Bigg], \end{aligned} \tag{22}$$

where

- $z(y_j)$: The distance between the scanning plane and the book surface (see Fig. 2). That is, $z(y_j)$ is the practical representation of $\boldsymbol{s}$. $z(y_j)$ is represented as follows:

$$z(y_j) = \sum_{y_k=y_0}^{y_j} \tan\theta(y_k) \quad (0 < y_j < y_0), \tag{23}$$

  where $\theta(y_j)$ is the slant angle of the book surface. That is, $\theta(y_j)$ is the practical representation of φ and Eq. (23) corresponds to $\boldsymbol{s}(\varphi)$ in Eq. (15).
- $I_s(y, z, y_j)$: The illuminant intensity distribution on the y-z plane when taking the 1D image at y_j. That is, $I_s(y, z, y_j)$ is the practical representation of $I_s(\boldsymbol{s}(\boldsymbol{x}), \boldsymbol{l}(\boldsymbol{x}))$. Based on the directional linear light source model, $I_s(y, z, y_j)$ is represented as follows:

$$I_s(y, z, y_j) = \frac{I_D(\psi(y, z, y_j))}{\sqrt{(y - (y_j - d_1))^2 + (z + d_2)^2}} + I_e, \tag{24}$$

$$\psi(y, z, y_j) = \arctan\left(\frac{y - (y_j - d_1)}{z + d_2}\right), \tag{25}$$

  where $(y_j - d_1, -d_2)$ denotes the location of the light source on the y-z plane, $\psi(y, z, y_j)$ the angle between the vertical line and the light source direction, $I_D(\psi)$ the directional distribution of the illuminant intensity, and I_e the environment light intensity (see Fig. 2).
- $f(\boldsymbol{n}, \boldsymbol{l}, \boldsymbol{v})$: The reflectance property of the book surface. We employ Phong's model (Ballard and Brown, 1982) to represent both the diffuse and specular components of the reflected light:

$$f(\boldsymbol{n}, \boldsymbol{l}, \boldsymbol{v}) = s\cos\varphi(\boldsymbol{n}, \boldsymbol{l}) + (1 - s)\cos^n\delta(\boldsymbol{n}, \boldsymbol{l}, \boldsymbol{v}), \tag{26}$$

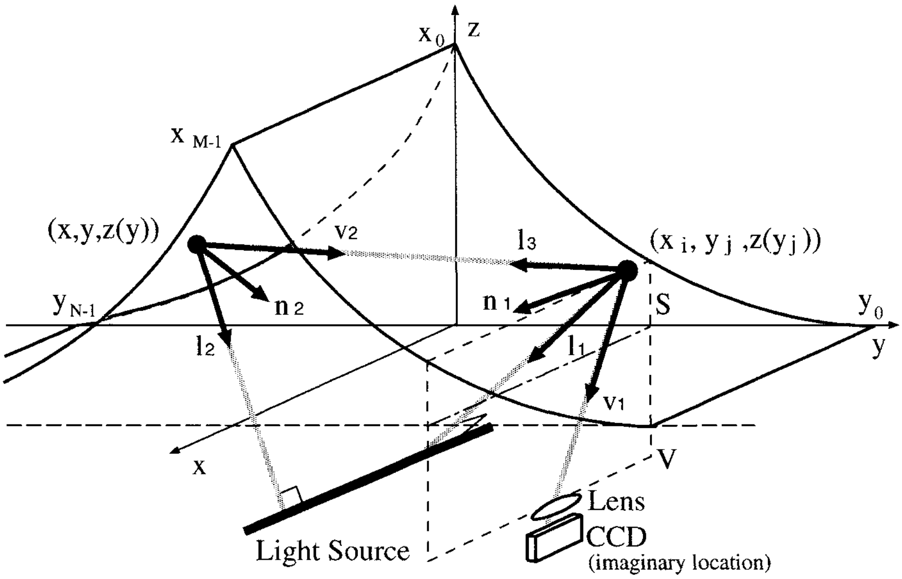

Figure 3. Interreflections on book surface.

where $\boldsymbol{n}$ denotes the surface normal, $\boldsymbol{l}$ the direction of the illumination, and $\boldsymbol{v}$ the view point direction. $\boldsymbol{n}$, $\boldsymbol{l}$, $\boldsymbol{v}$ are corresponding to $\boldsymbol{n}_1$, $\boldsymbol{l}_1$, $\boldsymbol{v}_1, \ldots,$ etc. as shown in Fig. 3. φ denotes the angle between $\boldsymbol{n}$ and $\boldsymbol{l}$, and δ the angle between $\boldsymbol{v}$ and the direction of the regular reflection. s and n specify the reflectance property.

- A: The area size of a pixel in the image.
- $V(y_n, y_j)$ (the visibility function): If the light reflected at $(x_m, y_n, z(y_n))$ can reach $(x_i, y_j, z(y_j))$, then this function takes 1, otherwise 0.

In the experiments, the parameters α, β, d_1, d_2, I_e, s, n, and $I_D(\psi)$ are estimated a priori using calibrated images of white flat slopes with known slants.

Since most of the book surface has the unprinted white background, we can assume that pixel values $P^*_w(y_j)$ corresponding to the background can be obtained from the observed image $P^*(x_i, y_j)$ as the maximum along each row y_j:

$$P^*_w(y_j) = \max_{x_i} P^*(x_i, y_j). \tag{27}$$

The optical model of the white background with the constant albedo ρ_w is represented as follows:

$$P_w(y_j) = \alpha\rho_w\{I_{\text{dir}}(x(y_j), y_j) + I_{\text{inter}}(x(y_j), y_j)\} + \beta, \tag{28}$$

where $x(y_j)$ denotes the location of the white background at y_j, and ρ_w can be computed at the ends of the book surface.

5. Shape Reconstruction

Under the practical conditions described in the previous section, the problem now becomes that of estimating the shape $\theta(y_j)$, the depth $z(y_j)$ and the albedo $\rho(x_i, y_j)$ which minimize the total error between the observed image intensity $P^*(x_i, y_j)$ and the image intensity model $P(x_i, y_j)$ represented by Eq. (20). The depth $z(y_j)$ can be calculated from $\theta(y_j)$ by Eq. (23) and the albedo $\rho(x_i, y_j)$ from $\theta(y_j)$, $z(y_j)$ and $P^*(x_i, y_j)$ by Eq. (20). Hence, the problem is essentially equivalent to estimating optimal $\theta(y_j)$ which minimize the total error.

This estimation problem can be formulated as a nonlinear optimization problem in N-dimensional space, where N represents the number of sampling points along the y-axis. To compute the numerical solution of this problem, simultaneous equations with an $N \times N$ coefficient matrix must be solved iteratively. In practice, however, there are thousands of sampling points, and hence, such a naive computation becomes extremely expensive. Moreover, local noise in an image introduces errors into $\theta(y_j)$, which are accumulated by Eq. (23) and lead to global errors in $z(y_j)$. The solution is detailed in the next section.

5.1. *Piecewise Shape and Albedo Approximation*

To improve the computational efficiency and the stability, we employ the following two piecewise approximations of the book surface:

1. 2*D Piecewise Polynomial Model Fitting*: Represent the 2D cross section by m quadratic polynomials. The y axis is partitioned into m uniform intervals and the depth $Z_p(y)$ at y in the pth interval is represented as follows:

$$Z_p(y) = \frac{z'_p - z'_{p-1}}{2\left(y_p^{\Delta} - y_{p-1}^{\Delta}\right)}\left(y - y_{p-1}^{\Delta}\right)^2 + z'_{p-1}\left(y - y_{p-1}^{\Delta}\right) + z_{p-1}, \quad (29)$$

   where y_p^{Δ} $(p = 0, 1, \dots, m)$ denotes the end point of a uniform interval of Δ pixels $(y_p^{\Delta} = y_{p\times\Delta})$, $z_p = z(y_p^{\Delta})$, $z'_p = 2(z_p - z_{p-1})/(y_p^{\Delta} - y_{p-1}^{\Delta}) - z'_{p-1}$ and $z_0 = z'_0 = 0$ (just on the scanning plane). By using this model, the number of parameters to describe the cross section shape is reduced to m, also z_p can be regarded as the independent parameter of this problem instead of θ_i.
2. 3*D Tessellation of the Book Surface*: Approximate the 3D book surface by piecewise planar rectangles with constant albedos. Using this approximation, the computation time of $I_{\text{inter}}(x_i, y_j)$ can be reduced.

5.2. *Shape Recovering Algorithm*

We use the following iterative algorithm to recover the cross section shape of the book surface:

Step 1. Extract P_w^* and compute ρ_w from P^*. Also, estimate the initial shape by using the optical model ignoring $I_{\text{inter}}(x_i, y_j)$ in Eq. (20).[8]
Step 2. Recover the albedo distribution $\rho(\boldsymbol{x})$ using the initial shape and the observed image $P^*(x_i, y_j)$.
Step 3. Calculate $I_{\text{inter}}(x_i, y_j)$ using the tessellated book surface model.
Step 4. Calculate the depth z_p which minimize the total square error between P_w and P_w^* for the $I_{\text{inter}}(x_i, y_j)$ obtained at Step 3.
Step 5. Recover the albedo distribution $\rho(\boldsymbol{x})$ using the 3D shape estimated at Step 4, the $I_{\text{inter}}(x_i, y_j)$ obtained at Step 3 and $P^*(x_i, y_j)$.
Step 6. If the values z_p converge, then the algorithm is terminated. Otherwise go to Step 3.

The computation of z_p is realized by Method 1 followed by Method 2.

Method 1. Calculate z_p sequentially by minimizing the function G in each interval:

$$G(p, z_p) = \sum_{y_j = y_{p-1}^{\Delta}}^{y_p^{\Delta}} \{P_w^*(y_j) - P_w(y_j)\}^2. \quad (30)$$

Method 2. Calculate all z_p simultaneously by minimizing the function

$$H(z_1, \dots, z_m) = \sum_{p=1}^{m} G(p, z_p). \quad (31)$$

The results of Method 1 are used as the initial estimates of z_p.

6. Experiments

First, we show the experimental result of the shape estimation and the image restoration of a real book surface. Figure 4 shows an image of a real book surface taken by the image scanner described above and Fig. 5 is the intensity profile $P_w^*(y)$ of the white background. Note that due to oblique illumination (Fig. 3) the profile is not symmetric. Figure 6 shows the estimated cross-section shapes. The thin line denotes the initial estimation and the bold line the final result. The optimal number of polynomials obtained by the MDL criterion was 13 for $y < 0$ and 6 for $y > 0$. The book surface was tessellated by 20×20 (400) rectangles per side. Seven iterations are required to obtain this shape.

Figure 7 shows the image restored using the estimated shape. The restored image is generated by the estimated albedos. For the fine restoration, we applied the following methods:

1. Enhance the contrast between the albedos at printed and unprinted areas.
2. Interpolate the albedos by cubic convolution.
3. Remove the shading along the x-axis caused by the limited length of the light source.

One can confirm that the readability of the book surface is drastically improved by the image restoration. This result demonstrates that the shape is accurately estimated enough for the image restoration task. Next, we show the experimental results using an artificial 3D

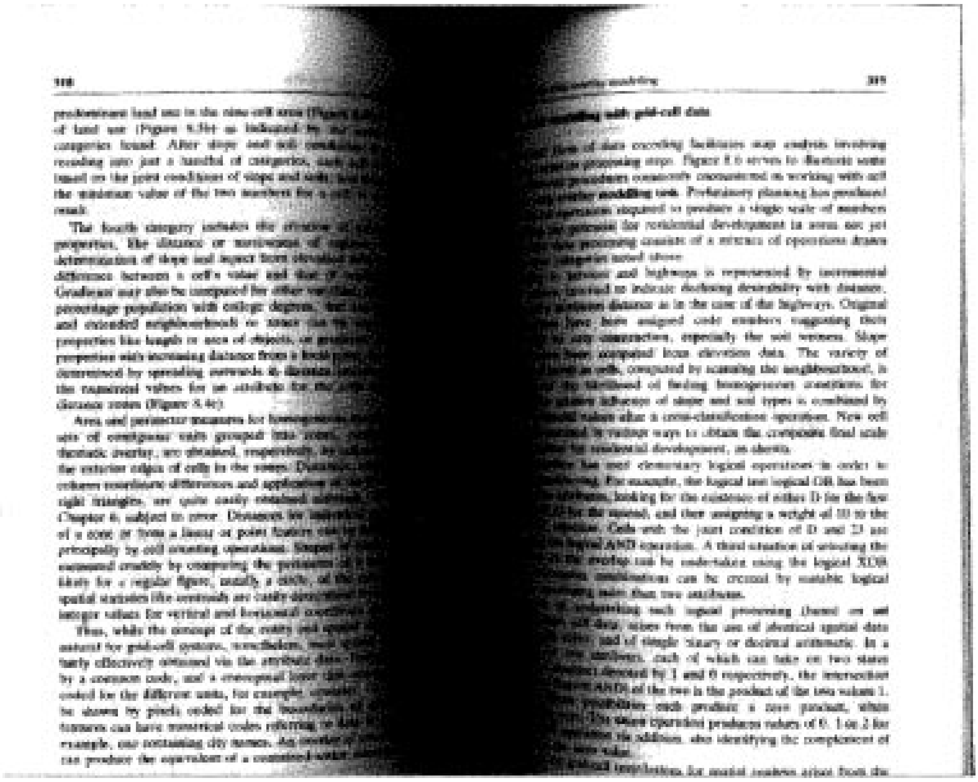

Figure 4. Observed image.

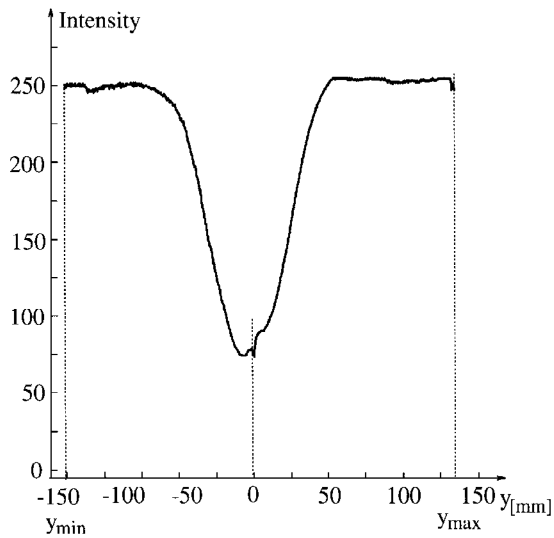

Figure 5. Image intensity of background paper.

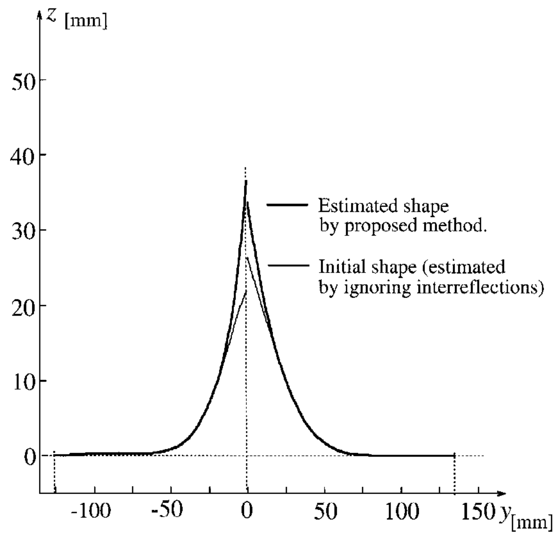

Figure 6. Estimated shapes.

model with a known shape to demonstrate the effectiveness and accuracy of the proposed algorithm.

Table 1 shows the computation time (on a SPARC Station 10) and the mean error of the estimation using the piecewise polynomial model fitting and the full pointwise estimation[9]. This result demonstrates that the piecewise shape approximation drastically reduces the computation time. Moreover, the accuracy of the estimation is improved, because the piecewise approximation provides stability against noise.

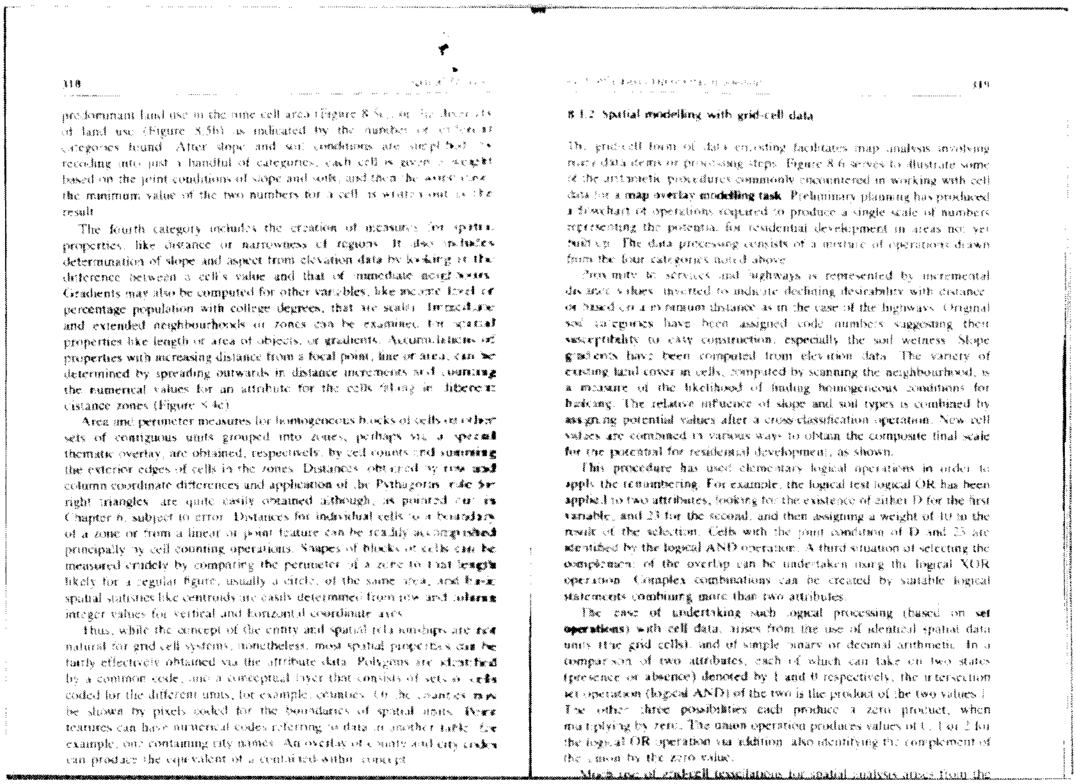
318

predominant land use in the nine cell area (Figure 8.5a), or the diversity of land use (Figure 8.5b) as indicated by the number of different categories found. After slope and soil conditions are simplified by recoding into just a handful of categories, each cell is given a weight based on the joint conditions of slope and soils, and then the [illegible] the minimum value of the two numbers for a cell is written out as the result.

The fourth category includes the creation of measures for spatial properties, like distance or narrowness of regions. It also includes determination of slope and aspect from elevation data by looking at the difference between a cell's value and that of immediate neighbours. Gradients may also be computed for other variables, like income level or percentage population with college degrees, that are scalar. Immediate and extended neighbourhoods or zones can be examined for spatial properties like length or area of objects, or gradients. Accumulations of properties with increasing distance from a focal point, line or area, can be determined by spreading outwards in distance increments and counting the numerical values for an attribute for the cells falling in different distance zones (Figure 8.4c).

Area and perimeter measures for homogeneous blocks of cells or other sets of contiguous units grouped into zones, perhaps via a special thematic overlay, are obtained, respectively, by cell counts and summing the exterior edges of cells in the zones. Distances obtained by row and column coordinate differences and application of the Pythagoras rule for right triangles are quite easily obtained although, as pointed out in Chapter 6, subject to error. Distances for individual cells to a boundary of a zone or from a linear or point feature can be readily accomplished principally by cell counting operations. Shapes of blocks of cells can be measured crudely by comparing the perimeter of a zone to that length likely for a regular figure, usually a circle, of the same area, and basic spatial statistics like centroids are easily determined from row and column integer values for vertical and horizontal coordinate axes.

Thus, while the concept of the entity and spatial relationships are not natural for grid cell systems, nonetheless, most spatial properties can be fairly effectively obtained via the attribute data. Polygons are identified by a common code, and a conceptual layer that consists of sets of cells coded for the different units, for example, counties. Or the counties may be shown by pixels coded for the boundaries of spatial units. These features can have numerical codes referring to data in another table, for example, one containing city names. An overlay of county and city codes can produce the equivalent of a contained-within concept.

319

8.1.2 Spatial modelling with grid-cell data

The grid-cell form of data encoding facilitates map analysis involving many data items or processing steps. Figure 8.6 serves to illustrate some of the arithmetic procedures commonly encountered in working with cell data for a **map overlay modelling task**. Preliminary planning has produced a flowchart of operations required to produce a single scale of numbers representing the potential for residential development in areas not yet built up. The data processing consists of a mixture of operations drawn from the four categories noted above.

Proximity to services and highways is represented by incremental distance values, inverted to indicate declining desirability with distance, or based on a maximum distance as in the case of the highways. Original soil categories have been assigned code numbers suggesting their susceptibility to easy construction, especially the soil wetness. Slope gradients have been computed from elevation data. The variety of existing land cover in cells, computed by scanning the neighbourhood, is a measure of the likelihood of finding homogeneous conditions for building. The relative influence of slope and soil types is combined by assigning potential values after a cross-classification operation. New cell values are combined in various ways to obtain the composite final scale for the potential for residential development, as shown.

This procedure has used elementary logical operations in order to apply the renumbering. For example, the logical test logical OR has been applied to two attributes, looking for the existence of either D for the first variable, and 23 for the second, and then assigning a weight of 10 to the result of the selection. Cells with the joint condition of D and 23 are identified by the logical AND operation. A third situation of selecting the complement of the overlap can be undertaken using the logical XOR operation. Complex combinations can be created by suitable logical statements combining more than two attributes.

The ease of undertaking such logical processing (based on **set operations**) with cell data, arises from the use of identical spatial data units (the grid cells), and of simple binary or decimal arithmetic. In a comparison of two attributes, each of which can take on two states (presence or absence) denoted by 1 and 0 respectively, the intersection set operation (logical AND) of the two is the product of the two values 1. The other three possibilities each produce a zero product, when multiplying by zero. The union operation produces values of 0, 1 or 2 for the logical OR operation via addition, also identifying the complement of the union by the zero value.

Figure 7. Restored image.

Table 1. Effectiveness of the piecewise polynomial model fitting.

	Number of parameters	Time: Ratio	Time: (Real [min])	Error [mm]
Piecewise	15	1	(1.18)	0.94
Pointwise	480	233	(276.17)	1.28

Table 2. Effectiveness of the tessellated book surface.

n	Number of rectangles	Time: Interreflections ratio	(real [sec])	Time: Reconstruction ratio	(real [min])	Error [mm]
1	2	0.0026	(0.07)	2.9	(1.3)	22.04
5	50	0.028	(0.76)	3.7	(1.7)	3.46
10	200	0.11	(2.90)	3.1	(1.5)	2.19
20	800	0.43	(11.8)	4.4	(2.1)	2.03
40	3200	1.67	(46.2)	11.4	(5.4)	2.16
Point-wise	628145	100.0	(2735.5)	100.0	(47.1)	2.35

Table 2 shows the computation times and the mean errors for a $n \times n$ tessellation of the book surface. We notice that tessellation with an adequate number of rectangles, such as $n = 20$, greatly reduces the computation time while maintaining the accuracy of the result. In this case, the estimated shape is as accurate as the pointwise case (the lowest column in Table 2).

7. Conclusions

In this paper, we discussed the real world shape-from-shading problem recovering the 3D shape of the book surface from a scanner image. We introduced special constraints which are necessary to solve the shape-from-shading problem with interreflections under a proximal light source. In our problem, however, these assumptions are not artificial but natural. Hence, our problem can be solved without introducing imaginary assumptions. It was shown that this problem can be solved by an iterative non-linear optimization to estimate the mutually dependent parameters: shape, depth and albedo. To improve the efficiency and stability, we employed piecewise approximations of the shape and the albedo distribution. Experimental results demonstrated that the proposed algorithm can recover the 3D shape accurately and efficiently enough for the restoration of the distorted book image.

The current method has the limitations that the center line separating book pages must be aligned parallel to the x-axis, and the reflectance property of the book surface must be known. Generalizing our method to remove these limitations will greatly improve its value in practical applications.

Notes

1. ρI_s can be determined assuming that $\varphi(\boldsymbol{x})$ is equal to zero at $\boldsymbol{x}$ where $I_o(\boldsymbol{x})$ takes the maximum value.
2. As will be described in later, the light source of the image scanner moves synchronously with the scanning sensor, i.e., observation location.
3. Unfortunately, the algebraic representation of ρ cannot be obtained from Eq. (13), because the left side ρ also appears in right side as an argument of I_{inter} which is a non-linear function of $\boldsymbol{s}$, φ and ρ. (See Eq. (11).)
4. The ruled surface is generated by sweeping a straight line passing across a curve $\boldsymbol{s}(\boldsymbol{x}(u))$. The ruled surface includes varieties of surfaces: hyperboloid of one sheet, hyperbolic paraboloid, cylindrical surface, conical surface, $\ldots$, etc.
5. $\boldsymbol{s}_u$ can be the independent argument of I_o instead of φ_u. Since, the choice of the independent argument does not effect the context hereafter, we employ φ_u.
6. The uniqueness in the shape from shading with interreflections has not been proven yet. It is an open problem in Computer Vision.
7. Cylindrical surface is one of the ruled surface described in Section 3.1.
8. In this estimation, the optimal number of intervals m is also calculated based on the MDL criterion (Rissanen, 1978).
9. In this experiment, half of the 3D model ($y > 0$) is used so the interreflections are ignored.

References

Asada, M. 1987. Cylindrical shape from contour and shading without knowledge of lighting conditions or surface albedo. *Proc. of ICCV*, pp. 412–416.

Ballard, H.D. and Brown, C.M. 1982. *Computer Vision*. Prentice Hall Inc.: Englewood Cliffs, New Jersey, pp. 93–102.

Horn, B.K.P. 1975. Obtaining shape from shading information. *The Psychology of Computer Vision*, P.H.Winston (Ed.), McGraw-Hill Book Co.: New York, pp. 115–155.

Ikeuchi, K. 1982-07. Determining 3D shape from shading information based on the reflectance map technique. *Trans. IECE Japan, Part D*, J65-D(7):842–849.

Nayar, S.K., Ikeuchi, K., and Kanade, T. 1990. Shape from interreflections. *ICCV*, pp. 2–11.

Rissanen, J. 1978. Modeling by shortest data description. *Automatica*, 14:465–471.

Tikhonov, A.N. and Arsenin, V.Y. 1977. *Solutions of Ill-Posed Problems*. Winston: Washington, DC.

Woodham, R.J. 1981. Photometric method for determining surface orientation from multiple images. *Opt. Eng.*, 19(1):139–144.